Transmembrane Pores Formed by Human Antimicrobial Peptide LL-37

Chang-Chun Lee,[†] Yen Sun,[†] Shuo Qian,[‡] and Huey W. Huang[†*]

[†]Department of Physics and Astronomy, Rice University, Houston, Texas; and [‡]Center for Structural Molecular Biology and Chemical Sciences Division, Oak Ridge National Laboratory, Oak Ridge, Tennessee

ABSTRACT Human LL-37 is a multifunctional cathelicidin peptide that has shown a wide spectrum of antimicrobial activity by permeabilizing microbial membranes similar to other antimicrobial peptides; however, its molecular mechanism has not been clarified. Two independent experiments revealed LL-37 bound to membranes in the α-helical form with the axis lying in the plane of membrane. This led to the conclusion that membrane permeabilization by LL-37 is a nonpore carpet-like mechanism of action. Here we report the detection of transmembrane pores induced by LL-37. The pore formation coincided with LL-37 helices aligning approximately normal to the plane of the membrane. We observed an unusual phenomenon of LL-37 embedded in stacked membranes, which are commonly used in peptide orientation studies. The membrane-bound LL-37 was found in the normal orientation only when the membrane spacing in the multilayers exceeded its fully hydrated value. This was achieved by swelling the stacked membranes with excessive water to a swollen state. The transmembrane pores were detected and investigated in swollen states by means of oriented circular dichroism, neutron in-plane scattering, and x-ray lamellar diffraction. The results are consistent with the effect of LL-37 on giant unilamellar vesicles. The detected pores had a water channel of radius 23–33 Å. The molecular mechanism of pore formation by LL-37 is consistent with the two-state model exhibited by magainin and other small pore-forming peptides. The discovery that peptide-membrane interactions in swollen states are different from those in less hydrated states may have implications for other large membrane-active peptides and proteins studied in stacked membranes.

INTRODUCTION

Human antimicrobial peptide (AMP) LL-37 is the most studied member of the cathelicidins (1), a major family of mammalian proteins that play various roles in host defense and inflammation (1–5). Considering its small size and relatively simple structure, it is remarkable that LL-37 contains all of the necessary information to perform its diverse functions, including antimicrobial activity, chemotactic effects that contribute to immune responses, release of inflammatory mediators, transcriptional responses, and wound healing (1,6). Most of these functions, with the exception of direct antimicrobial activity, require specific molecular interactions. Like all other AMPs (7), LL-37 is water-soluble, but it spontaneously binds to bacterial LPS and lipid bilayers (2) and permeabilizes microbial membranes, leading to rapid cell death (2,8). The question is, how does LL-37 permeabilize membranes? Previous experiments revealed LL-37 bound to lipid bilayers in the α-helical form (9) with the helical axis lying parallel to the plane of bilayer (8,10). On the basis of this finding, it is widely believed that LL-37 does not form pores in membranes but permeabilizes or destroys membranes by means of a nonpore carpet mechanism (8,9,11).

Here, we report the discovery of transmembrane pores induced by LL-37. The pore formation coincided with the detection of LL-37's helical axis oriented approximately normal to the plane of the membranes. The water channel

of the detected pores ranged from 23 to 33 Å in radius, depending on the peptide/lipid (P/L) ratio. We found out why previous investigations did not observe LL-37 inserted in membranes. In previous studies of peptide orientation that used solid-state NMR (10) or polarized Fourier-transform infrared spectroscopy (FTIR) (8), the membranes were prepared in multilayers. In commonly prepared membrane multilayers, the periodic spacing of bilayers (the D spacing) is up to ~52 Å at full hydration. Under such conditions, our measurements agreed with previous studies in which LL-37 helices were reported to be in the plane of the bilayers and no pores were detected (8,11). However, we found that LL-37 helices were oriented approximately normal to the plane of the bilayers when the D spacing exceeded ~70 Å. For multilayers, this was a condition with excessive water, i.e., a swollen state. It was as if the D spacing had to substantially exceed the length of the peptide (~37 × 1.5 or 55 Å, assuming a helix (9)) before LL-37 could be found inserted in the membranes.

We investigated multilayers in swollen states using x-ray diffraction to make sure that the lipid-peptide bilayers were in the lamellar phase. The thermal fluctuations of bilayers in swollen lamellar states are of theoretical interest in statistical physics (12,13). Therefore, they have been extensively analyzed with the use of x-ray diffraction (13–15) and are now well understood. We used the method of oriented circular dichroism (OCD) (16) to measure the peptide orientation in swollen states, and used neutron in-plane scattering to detect and measure the transmembrane pores induced by LL-37. We then correlated the results with the kinetic effect of LL-37 binding to giant unilamellar vesicles (GUVs). We

conclude that the membrane permeabilization mechanism of LL-37 is consistent with the two-state model exhibited by other well-studied pore-forming peptides (17,18).

MATERIALS AND METHODS

Materials

Human LL-37 (LLGDF FRKSK EKIGK EFKRI VQRIK DFLRN LVPRT ES) was synthesized by GenScript USA (Piscataway, NJ) to >95% purity by high-performance liquid chromatography. We purchased 1,2-dioleoyl-sn-glycero-3-phosphocholine (DOPC) and 1,2-dioleoyl-sn-glycero-3-phosphoethanolamine-N-(lissamine rhodamine B sulfonyl) (Rh-DOPE) from Avanti Polar Lipids (Alabaster, AL). Calcein was purchased from Invitrogen (Carlsbad, CA). Other chemicals were purchased from Sigma-Aldrich (St. Louis, MO). All materials were used as delivered.

Stacked membranes

Open stacked membranes were prepared as previously described (19). Briefly, a mixture of LL-37 and DOPC (in molar ratios of P/L = 1/100, 1/80, or 1/50) in organic solvent (1:1 (v/v) chloroform and tetrafluoroethylene) was directly deposited onto a cleaned quartz plate, dried under vacuum, and then hydrated by water vapor (referred to as open samples, each with 0.2–0.4 mg of lipid). X-ray diffraction indicated that the multiple bilayers were well aligned parallel to the substrate. The sample was kept in a temperature-humidity chamber as previously described (20). A temperature transducer and a relative humidity (RH) sensor were mounted close to the sample to monitor the sample condition. The outputs from the sensing elements were fed to PID feedback control circuits, which in turn powered two sets of Peltier modules (one to heat or cool the sample, and one to heat or cool a water reservoir). Once the humidity sensor reached a new hydration level, the sample equilibration time was at most a couple of minutes (as determined by continuous x-ray scanning). For data acquisition, we allowed at least 10 min for equilibration.

For neutron experiments that required a large amount of sample (~30 mg of lipid), we used stacked membranes sandwiched between two quartz plates as described previously (21). Briefly, the peptide-lipid mixture was first lyophilized and then hydrated by 100% RH water vapor overnight to a gel-like texture at ~35°C. The gel-like mixture was spread on one quartz plate and then covered by a second plate (referred to as sandwiched samples at full hydration). For swollen-state samples, an amount of water equal to the lipid in weight was added to the fully hydrated peptide-lipid mixture, covered by a second substrate, and equilibrated for 1 h or longer (referred to as sandwiched samples in a swollen state). Double substrates have been shown to be capable of aligning thick lipid multilayers (22). The membrane alignment in a sandwiched sample can be examined by polarized microscopy (21,22) or neutron diffraction, or by x-ray diffraction if one substrate is replaced by a mylar sheet.

OCD

CD spectra were measured in a Jasco (Tokyo, Japan) J-810 spectropolarimeter. For the OCD measurements, the substrates of stacked membranes were oriented normal to the incident light (16). A detailed analysis of OCD for α-helices, including its experimental verification and limitations, has been provided elsewhere (16). The technique has also been independently confirmed by other laboratories (23–25). For practical purposes, the CD of helices in solution can be recognized by a positive ~190 nm peak, a negative ~208 nm peak, and a negative ~224 nm peak. The OCD of a helix perpendicular to the incident light (parallel to the plane of the membrane) is similar to the solution CD except that it has a stronger negative 208 nm peak. In comparison with the solution helical CD, the OCD of a helix

parallel to the incident light (normal to the plane of the membrane) has the positive peak red-shifted, no peak at 208 nm, and a smaller 224 nm negative peak. As a result, the zero crossing point between the positive and negative peaks is also red-shifted. The vanishing of the negative peak at ~208 nm has a theoretical basis (i.e., the Moffitt theory (16)) and is the most prominent feature of a helix oriented in the direction of light (normal to the membrane).

Neutron in-plane scattering

Neutron experiments were performed at the HFIR Bio-SANS CG-3 station (26) of Oak Ridge National Laboratory. The small-angle scattering beamline was equipped with a 1×1 m area detector (5.1×5.1 mm^2 pixels) with an adjustable sample-to-detector distance of 1–15 m. The neutron wavelength was 6 Å with $\Delta\lambda/\lambda \sim 15\%$. The detector was positioned to record the q range from 0.013 to 0.3 Å^{-1}. Sandwiched samples were sealed in an aluminum holder that provided a beam path of 16 mm in diameter. The scattering data were collected for 10–30 min per sample. More technical details can be found in He et al. (21).

X-ray lamellar diffraction

Details regarding the equipment and experimental procedures used, as well as the data analysis for x-ray lamellar diffraction by multilayers, can be found elsewhere (27). The open sample was housed in a temperature-humidity chamber in which the hydration level of the sample was controlled by the RH of water vapor. The substrate orientation was vertical, and θ–2θ scans were recorded at a humidity level up to ~100% RH and at a few lower RH values. We used the hydration dependence to determine the diffraction phases according to the swelling method. The diffraction patterns at RH > ~98% suffered undulation damping. Thus, the patterns at ~98% RH were used to construct the electron density profiles across the bilayer.

Grazing-angle x-ray scattering for swollen samples

The equipment and experimental procedure used for grazing-angle scattering were as previously described (28). Swollen samples were sandwiched between a Si wafer and a mylar sheet. The sample was held horizontally and then tilted $\leq 0.5°$ for scanning. X-rays from a point source of Cu K$_\alpha$ radiation (operating at 35 mA/40 kV) were double-focused (by a pair of bent mirrors) horizontally at the sample. The scattering pattern was recorded by a CCD area detector (Gemstar HS 75; Photonic Science Ltd., E. Sussex, UK). The beam center and the sample-to-detector distance were determined by powder scattering from Ag-behenate.

GUV experiment

GUVs of DOPC plus 0.5 mol % Rh-DOPE were produced in 200 mM sucrose solution by electroformation (29). The osmolality of every solution used in the GUV experiment was measured by a Wescor model 5520 dew-point osmometer (Wescor, Logan, UT). The micropipettes and walls of the experimental chambers were coated with 1% bovine serum albumin to neutralize the charge on the bare glass surface and then washed extensively with water. All GUV experiments were performed at room temperature (~25°C).

For the leakage experiment, the solution in the GUV production chamber also contained 10 μM calcein. A small amount of the GUV suspension was transferred to an observation chamber containing 190 mM glucose, 10 mM HEPES at pH 7, and 5 μM LL-37. The GUVs settled at the bottom due to the density differential and were observed under an Olympus (Tokyo, Japan) microscope (model IX81) and recorded with a Hamamatsu Photonics (Hamamatsu City, Japan) digital CCD camera

(model C10600-10B). The content leakage was monitored by calcein fluorescence. At the end of the leakage, we used the lipid dye image to inspect the effect on the vesicle membrane.

For the aspiration experiments, a GUV was aspirated by a micropipette with a small constant sucking pressure (~100 Pa, producing a membrane tension of ~0.4 mN/m) and transferred via a transfer pipette (29) to an observation chamber containing 190 mM glucose, 10 mM HEPES at pH 7, and 0.5 μM LL-37. Equiosmolality between the inside and outside of the GUV was maintained throughout the experiment. To record the experiment, we used fluorescence imaging with a Photometrics (Tucson, AZ) coolSNAP HQ2 camera. The technical details of the aspiration experiment can be found elsewhere (29).

RESULTS AND ANALYSIS

OCD of LL-37 embedded in stacked membranes

The open sample was kept in a temperature-humidity chamber in which separate temperature controls were used for the sample and the water source (20). OCD was measured with the sample substrate oriented vertically, so that the UV beam for CD was incident perpendicular to the plane of the bilayers (16). By varying the temperature of the water source from below the sample temperature (20°C) to the same temperature, we were able to vary the humidity at the sample (measured by a humidity sensor in the vicinity of the sample) from ~70% to ~100% RH. In this range of RH, the spectrum was independent of RH (Fig. 1 A). The OCD indicated that the peptide helices were oriented approximately parallel to the plane of the bilayers (16). This result is consistent with previous measurements obtained by solid-state NMR (10) and polarized FTIR (8). X-ray diffraction of the sample showed that the D spacing increased from 47 Å at ~70% RH to 52 Å at ~100% RH (Fig. 2 A). The Bragg peaks at ~100% RH were broadened and diminished at high orders, indicating bilayer undulations in water (12,30).

We then set the water temperature to 1–2° above the sample temperature, which caused water vapor to condense on the sample. As the water visibly condensed on the sample, the surface of the sample slowly slid downward and out of the beam path (because the substrate was vertical). In the meantime, the OCD changed its shape with an overall decreasing amplitude (Fig. 1 A), indicating a decreasing amount of sample in the beam path, but an increasing fraction of the remaining peptide helices changed to perpendicular to the plane of the bilayers. Eventually, the OCD changed into a spectrum corresponding to all helices oriented approximately normal to the plane of the bilayers (16). At that moment, the humidity chamber was opened to expose the sample to the room air (~50% RH) and the sample was held horizontal for ~10 min. This stopped the sample from flowing, and the OCD changed back to the original spectrum of all helices parallel to membranes, but the amplitude was smaller than the original amplitude due to the partial loss of the sample. From the last two spectra, we obtained two mutually normalized OCD spectra
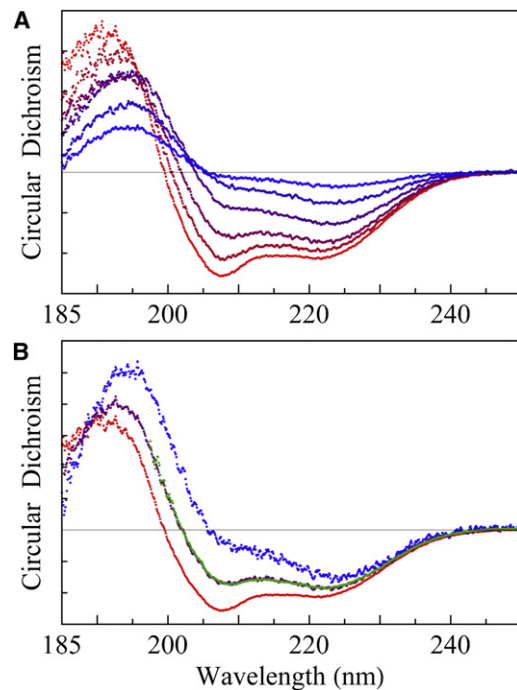
FIGURE 1   OCD. (*A*) Bottom red spectrum is the OCD of an open sample of P/L = 1/50, unchanged from 50% to 100% RH. As excessive water condensed on the sample, the spectrum gradually changed in time from bottom to top (the blue color content of the spectra increased with time), whereas the amount of sample in the CD beam path decreased because the surface of the sample slowly slid downward. It took 40 min of continuous OCD scanning from the red to the blue spectrum. The scan time for each spectrum was ~4 min, including the resetting time, at 1 nm bandwidth, 0.1 nm/point, and 20 nm/min scan rate. Ten spectra were taken, but for clarity only five are shown. (*B*) At the appearance of the top blue spectrum in *A* (rescaled in *B*), the sample was open to 50% RH and held horizontally for ~10 min. This made the sample stop flowing, and the spectrum turned to the bottom red curve. The blue and red spectra were obtained from the same amount of sample (*blue*, I spectrum for helices normal to the bilayers; *red*, S spectrum for helices parallel to the bilayers). The green spectrum was obtained from a sandwiched sample in a swollen state, fit by a linear combination of the I and S spectra (0.4 I + 0.6 S; *purple line*), indicating that 40% of the helices were oriented normal to the bilayers.

of the LL-37 helices: one oriented approximately parallel (the S spectrum) and one oriented approximately perpendicular (the I spectrum) to the plane of the membranes (Fig. 1 B). The same experiment was repeated several times for each P/L = 1/80 and 1/50 sample, with the same result.

The sandwiched samples used in the neutron experiments were too thick (~30 mg of lipid) for CD measurements. Therefore, we reproduced sandwiched samples for CD measurements with a smaller amount of lyophilized peptide-lipid mixture (~0.5 mg of lipid). Two different hydration conditions were used. In one case, the mixture was hydrated by ~100% RH and the measured OCD was the S spectrum, consistent with open samples hydrated by ~100% RH. In the other case (the swollen state), the lyophilized peptide-lipid mixture was equilibrated with the same weight of water as the amount of lipid. However, the second
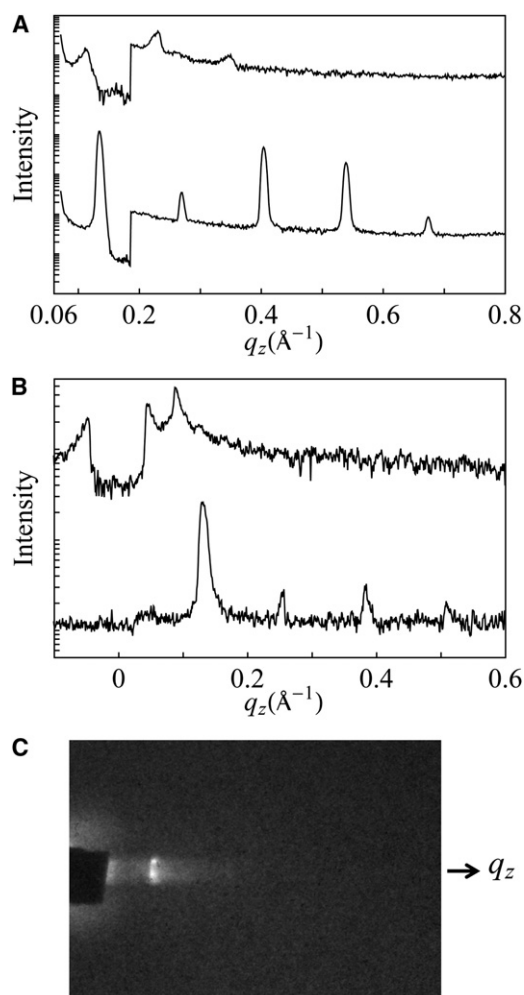
FIGURE 2   (A) X-ray lamellar diffraction by θ–2θ scan from an open sample of P/L = 1/50 equilibrating at 98% RH (*bottom*) and 100% RH (*top*; with an attenuator below $q = 0.19$ Å^{-1}). Note that at 100% RH, the peaks were strongly damped by layer undulations (30). (*B*) X-ray grazing-angle scattering from an open sample of P/L = 1/50 equilibrated at 60% RH (*bottom*) and (*top*) in a swollen state (covered by a mylar sheet; also with an attenuator below $q = 0.04$ Å^{-1}). Note that in the swollen state, the first-order peak has the characteristic power-law line shape as predicted by Caillé's theory (12,14) due to layer undulations in the swollen lamella. (*C*) Grazing-angle scattering from the swollen lamella (*B*) recorded on the CCD detector, which was oriented with the *z* axis vertically up. The beam center was at the baseline. The rectangular diffraction peak image was the shape of the x-ray beam cross section. The intensity profile along the *z* axis is shown at the top of panel *B*.

cover, in the effort to avoid air bubbles in the sandwiched sample, inevitably applied pressure and squeezed out a small but unknown amount of water from the holder, despite the use of a spacer between the two substrates. It was difficult to reproduce the exact amount of water in the swollen state, but the water content was nevertheless precisely measured by its D spacing. In all swollen cases, the measured OCD was a linear combination of the S and I spectra (16), indicating that 30–60% of the LL-37 peptides were oriented perpendicular to the bilayers (one example is shown in

Fig. 1 *B*). It appeared that as long as the sample was in a swollen state, a substantial fraction of LL-37 peptides were oriented normal to the bilayers.

Previous solution CD studies on LL-37 indicated that the peptide is a random coil in water containing no salt (as in our stacked-membranes preparation) but changes to α-helical upon the introduction of lipid vesicles (2,10,31). Thus, it is clear that the LL-37 peptides in our stacked membranes were membrane-bound whether they were in nonswollen or swollen states, since the CD spectra were clearly those of α-helices. One important question is, how might the undulations of the bilayers in the swollen state have affected the orientation of the peptide? First, we examined the swollen state by x-ray diffraction (Fig. 2, *B* and *C*). In this case, the cover for the sandwiched sample was a mylar sheet that was transparent to x-ray. Fig. 2 *C* shows the scattering pattern of a lamellar phase (D spacing = 71 Å) in which the first-order peak has the characteristic power-law line shape (Fig. 2 *B*, *top*) as predicted by Caillé's theory (12–15). The undulations of bilayers in a swollen lamellar phase are well understood. The spectrum of out-of-plane undulations of bilayers is dominated by long wavelengths; therefore, despite the enhanced fluctuations induced by swelling, the dominant tilt angles are still small (12–15). The fact that the I spectrum was measured is proof that the bilayers were well aligned on average, and it can only be explained by the majority of helices being approximately normal to the plane of the lamellar phase (16).

To prove that the I and 40% I spectra in Fig. 1 *B* could not be the result of bilayer undulations with surface-bound helices, imagine that the bilayers had become vesicles (with the helices on the bilayer surface), then the CD spectrum would be the familiar CD of helices in solution, which is (1/3)I + (2/3)S (16). Thus, if the helices were on the bilayer surface, even the worst-case perturbation of bilayers could not produce the 40% I spectrum, not to mention the I spectrum.

According to a previous NMR study of LL-37 adsorbed on a lipid micelle (9), the membrane-bound LL-37 is largely α-helical with a bend in the helical axis at K12. Thus, it is similar to the melittin (32) and alamethicin (33) helixes, both of which exhibit the S and I states in membranes (16,34). Henzler Wildman et al. (10) performed oriented NMR on LL-37 in DMPC at P/L = 1/50 in stacked membranes prepared with 30 mol of H_2O per mole of lipid-peptide, but the exact hydration condition was unknown (most likely it was not in a swollen state, because the authors would have noted the sample flow problem). The authors concluded that the α-helix is oriented parallel to the surface of the bilayer (with a measured σ_{33}~10–25° relative to the surface). The first investigation of LL-37 orientation was performed by Oren et al. (8), who used polarized FTIR on stacked membranes of LL-37 in PC/cholesterol and PC/PG at P/L~1/70, hydrated with saturated D_2O vapor (a nonswollen state). The measured order parameter was consistent with helical axes parallel to the membrane surface.

Having broad spectra, CD is a low-resolution spectroscopy. It is an appropriate spectroscopic technique for fluid lipid systems in which structures are subject to significant fluctuations (e.g., in orientation) and thus have intrinsically low resolution, as shown by previous solid-state NMR measurements (10). Within the spectral resolution, the I spectrum is consistent with the great majority of helices approximately oriented normal to the plane of the membranes, and the S spectrum is consistent with the great majority approximately oriented parallel to the plane of the membranes, as dictated by Moffitt's theory (16). The exact orientations of the I and S states are not essential to our conclusion. What is essential is that we detected two distinct orientation states (one approximately parallel and one approximately normal to the plane of membranes) and, furthermore, the detection of the I state was coincidental with the detection of pores and no pores were detected in the S state (see below). As pointed out by Wu et al. (16), OCD cannot distinguish whether an intermediate state between I and S (such as the 40% I spectrum in Fig. 1 B) is due to uniformly tilted helices or due to a mixture of two distinct orientation states. For instance, one could interpret the series of intermediate states in Fig. 1 A as helices being uniformly stabilized in a series of tilt angles. However, this is physically unlikely and has never been observed in any peptide. It is more reasonable to assume that the intermediate spectrum in Fig. 1 B represents a mixture of helices in the S and I states.

Neutron in-plane scattering

The neutron in-plane scattering technique makes use of the large difference (contrast) between the neutron scattering by hydrogen and deuterium. We exchanged the water in our multilayer samples to D_2O by exposing the samples to D_2O vapor. Then, in the plane, the bilayers had a uniform scattering density, except for the D_2O channels in the transmembrane pores, as long as the magnitude of the scattering vector q was $<2\pi/(4.5 \text{ Å})$ (the denominator is the size of the cross section of a hydrocarbon chain) (21). Thus, if the peptides were to form pores in the membrane, neutron in-plane scattering would detect a collection of D_2O channels representing the pores diffusing in a two-dimensional uniform background (21).

We used a stack of three sandwiched samples, each containing 8–10 mg of lipid, for neutron scattering. The substrates were aligned perpendicularly to the incident neutron beam. The scattering vector q at small-angle scattering ($q < 0.3 \text{ Å}^{-1}$) was essentially in the plane of the aligned multilayers. Each sample was scanned in three conditions in the following sequence: 1), the sample was equilibrated with 100% RH D_2O vapor; 2), the sample was equilibrated in a swollen condition with a 1:1 (w/w) D_2O/lipid ratio; and 3), the sample was equilibrated in a swollen condition with H_2O. The results for P/L = 1/50

are shown in Fig. 3. The sample in the first condition showed only a lamellar peak at $q = 0.124 \text{ Å}^{-1}$ corresponding to a D spacing of 51 Å, the same as for open samples measured by x-ray in the same hydration condition. The lamellar peak was due to oily streak defects in multilayers (21,22). The absence of any other scattering signal indicated that there were no pores in the bilayers. In the second condition, there was a broad peak at 0.041 Å^{-1} and a shoulder peak at 0.085 Å^{-1}. The shoulder peak, which also appeared in other samples in swollen conditions with D_2O, was a lamellar peak resulting from oily streak defects corresponding to a D spacing of 74 Å. Both peaks disappeared in the third condition.

The broad peak at 0.041 Å^{-1} was due to the presence of D_2O columns in the membranes, and thus implied the presence of transmembrane pores. The peak disappeared upon exchange to H_2O as expected, since H_2O columns in membranes had no significant contrast against the lipid background by neutron scattering. Similar neutron in-plane scattering peaks induced by magainin, alamethicin, protegrin, and melittin were thoroughly studied in previous works (21,35–37). It was demonstrated that in some lipids, these peaks can be crystallized into a rhombohedral lattice (28) and are therefore amenable to x-ray diffraction analysis (38,39). The structures revealed by diffraction were indeed transmembrane pores (38,39).

The in-plane scattering intensity $I(q)$ is theoretically expressed as $I(q) = A|F(q)|^2 S(q)$, where $F(q)$ is the form factor, i.e., the scattering amplitude of an individual pore; $S(q) = \langle \sum_{i,j} exp[-i\boldsymbol{q}\cdot(\boldsymbol{r}_i - \boldsymbol{r}_j)]\rangle/N$ is the structure factor, where $\boldsymbol{r}_i$ is the position of the center of a pore in the plane of bilayer, $<>$ represents the ensemble average, N is the total number of pores; and A is the normalization constant. The analysis of neutron in-plane scattering was described in detail in a previous study (21), which showed that $F(q)$ is dominated by the scattering amplitude of the D_2O channel inside the pore, and therefore is essentially determined by
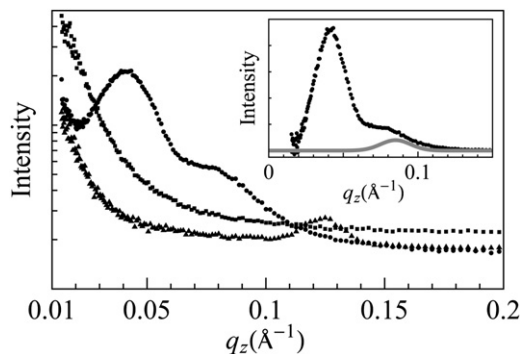

FIGURE 3   Neutron in-plane scattering of a sandwiched sample of P/L = 1/50 under three conditions: equilibrated at 100% RH D_2O (triangles), equilibrated with excessive D_2O in a swollen state (circles), and equilibrated with excessive H_2O in a swollen state (squares). Inset: Obtained from the circles curve after removing the background (the empty sample cell). The shoulder peak was fit with a Gaussian curve (gray) at 0.085 Å^{-1}.

the radius of the cylindrical D_2O channel. $S(q)$ can be simulated by randomly distributed disks on a plane representing pores in the bilayer. The peak comes from the interference due to nonoverlapping between disks. Therefore, the diameter of the disk represents the collision distance between two pores in the membrane. We carried out the fit to the data by adjusting three independent parameters: 1), the disk diameter, which is essentially determined by the position of the peak; 2), the fit to the left side of the peak, which is essentially determined by the density of the disks in the plane (which is the density of the pores in the membrane); and 3), the fit to the right side of the peak, which is essentially determined by the form factor $F(q)$ or the radius of the water channel.

The results obtained by the minimum χ^2 fit are shown in Fig. 4. At P/L = 1/50, the water channel radius is 33 Å and the collision distance (i.e., the closest approach between two pores) is 130 Å. At P/L = 1/100, the water channel radius is 23 Å and the collision distance is 82 Å. In comparison, the water channels of magainin pores are 15–25 Å in radius, with a collision distance of 70–84 Å (35). In one measurement, the melittin pores had a water channel of radius 21 Å and collision distance of 77 Å (34). The previous results, particularly for magainin, were obtained by repeated measurements with different P/L ratios and lipid compositions (35,37). Therefore, the pore radius range of 23–33 Å for LL-37 measured here should be regarded as a minimum range. Perhaps not surprisingly, the pores induced by LL-37 are larger than those induced by smaller peptides

(i.e., magainin or melittin). The number of LL-37 peptides that participated in each pore was ~5, which we calculated by assuming that all peptides were in pore formation. The precise number was unknown because it depended on the fraction of the peptides oriented normal to the bilayers (as noted above, the neutron samples could not be directly measured by OCD). In comparison, the magainin pores were estimated to contain four to seven peptides in each pore (35).

X-ray lamellar diffraction in nonswollen conditions

X-ray diffraction was used to investigate the condition of lipid bilayers in stacked membranes for both the swollen (see the OCD section above) and nonswollen states. In the nonswollen states, LL-37 helices were parallel to the bilayers, as determined by OCD. We performed x-ray diffraction to investigate the effect of surface-bound LL-37 on the lipid bilayers. We constructed electron density profiles of DOPC bilayers containing LL-37 at P/L = 0, 1/80, and 1/50 from the lamellar diffraction patterns obtained at ~98% RH (Fig. 5). The profile peaks at the phosphate group on both sides of bilayer. Thus the peak-to-peak distance (PtP) can be used to measure the changes in the bilayer thickness (as explained previously (27), the peptides do not contribute to the x-ray profile). In similarity to previous
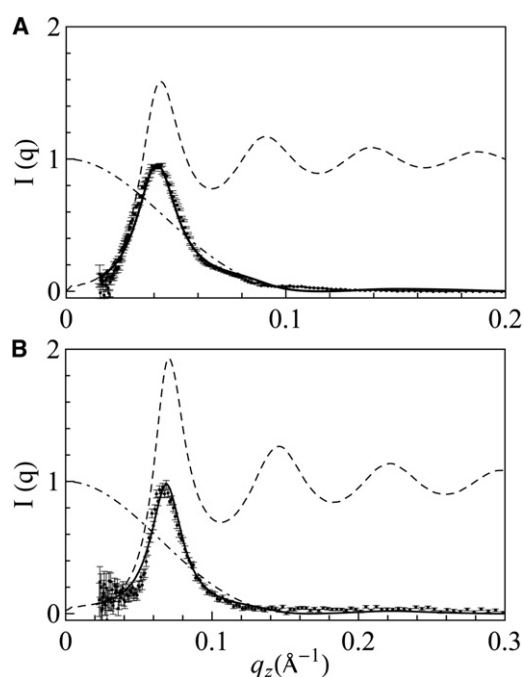

FIGURE 4 Analysis of neutron in-plane scattering. (A) P/L = 1/50 (data from Fig. 3, *inset*, after subtracting the shoulder peak). (B) P/L = 1/100. The dash-dotted curve is $|F(q)|^2$, the dashed curve is $S(q)$, and the solid curve is the minimum χ^2 fit.
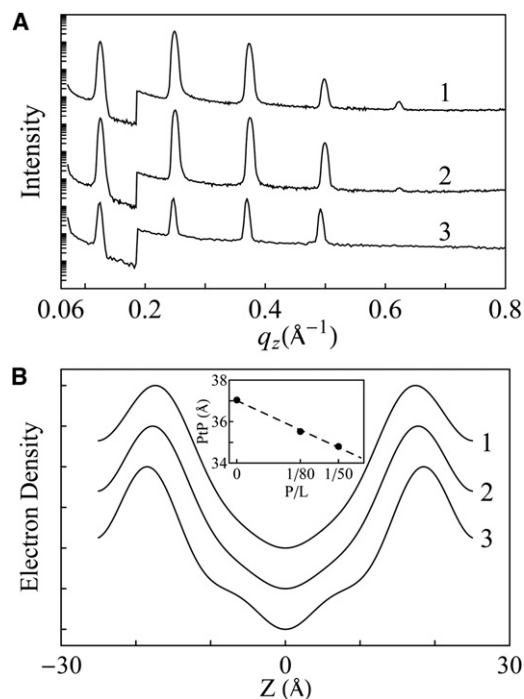

FIGURE 5 X-ray lamellar diffraction of open samples of 1), P/L = 1/50; 2), P/L = 1/80; and 3), pure DOPC (all at ~98% RH, 25°C). (A) Diffraction patterns. (B) Constructed electron density profiles across one unit cell (the coordinate z normal to the bilayer) from which the PtP was measured and plotted in the inset as a function of P/L.

measurements obtained with various peptides in their surface-bound states [17], we observed membrane thinning linearly proportional to P/L (Fig. 5). This membrane thinning effect by surface-bound peptides has also been detected by other techniques, such as atomic force microscopy on supported lipid bilayers [40] and small-angle x-ray scattering on lipid vesicles [41]. Our result is analyzed as follows: Let A_P be the monolayer area expansion per peptide embedded in the headgroup region of the monolayer, and A_L the cross section area per lipid. Then the fractional area expansion of the lipid monolayer (or the lipid bilayer) is $\Delta A/A = (P/L)(A_P/A_L)$. From the chain volume conservation, we have $\Delta A/A = -\Delta h/h = (P/L)(A_P/A_L)$, where the hydrocarbon thickness h is directly obtained from PtP by $h \approx PtP - 10$ Å [42]. Therefore, from the slope of the membrane-thinning data (Fig. 5), we obtain the value of $A_P = 309$ Å^2. This is not the along-the-axis cross section of the LL-37 helix. The peptide binding involves release of water molecules from the headgroup region, which makes A_P smaller than the physical size of the peptide [43].

Effect of LL-37 binding to GUVs

GUVs with lipid dye (red) in the bilayers and solution dye (green) in their contents were brought to a solution containing 5 μM LL-37. Leakage occurred stochastically (i.e., at random times) in individual GUVs, as observed in a previous magainin leakage experiment [44]. Fig. 6 A shows one example in which the content dye leaked out in ~200 s while the vesicle remained intact. This shows that the pores induced by LL-37 were stable (i.e., were not expanding indefinitely and did not disappear during the experimental time) and did not disintegrate the lipid vesicle.

The method of aspiration [45] allowed us to distinguish the surface binding from pore formation [18,29,46,47]. A GUV that formed in 200 mM sucrose solution was aspirated and brought to an isotonic glucose/HEPES solution containing 0.5 μM LL-37 (Fig. 6 B). The binding of the peptide initially expanded the protrusion inside the pipette, which allowed us to calculate the fractional area expansion $\Delta A/A$ [45]. The protrusion length reached a maximum and then began to decrease. This was the indication of pore formation in the membrane and the influx of the smaller sugar (glucose) molecules exceeding the outflow of the larger sugar (sucrose) molecules, resulting in an increase of the GUV volume [18,46]. The same experiment was repeated nine times with an average maximum $\Delta A/A = 1.3 \pm 0.7\%$.

DISCUSSION

The stability of the pores induced by LL-37 was demonstrated by the leakage experiment from GUVs. When a GUV was exposed to LL-37 in the solution, the dye inside the vesicle leaked out while the vesicle remained intact (Fig. 6). This indicated the formation of finite-sized pores in the membrane of GUV, which lasted for the entire experimental time. The same phenomena were previously observed by Tamba and Yamazaki [44] with magainin. This observation did not imply pore-size stability during the kinetic process. Recent kinetic studies showed that the pores induced by magainin and other pore-forming peptides initially leaked out large dye molecules but later leaked only smaller ones [48,49]. Whether LL-37 has similar pore-size kinetics remains to be investigated. None of these pore-forming peptides, including LL-37, dissolved the lipid bilayer as a detergent would.

The experiment with aspirated GUVs provided further insight into the process [18,29,46,47]. In this experiment, the amount of peptide bound to the GUV, or the P/L ratio, increased with time. The initial phase of LL-37 binding extended the protrusion length inside the micropipette, indicating a membrane area expansion of the GUV without
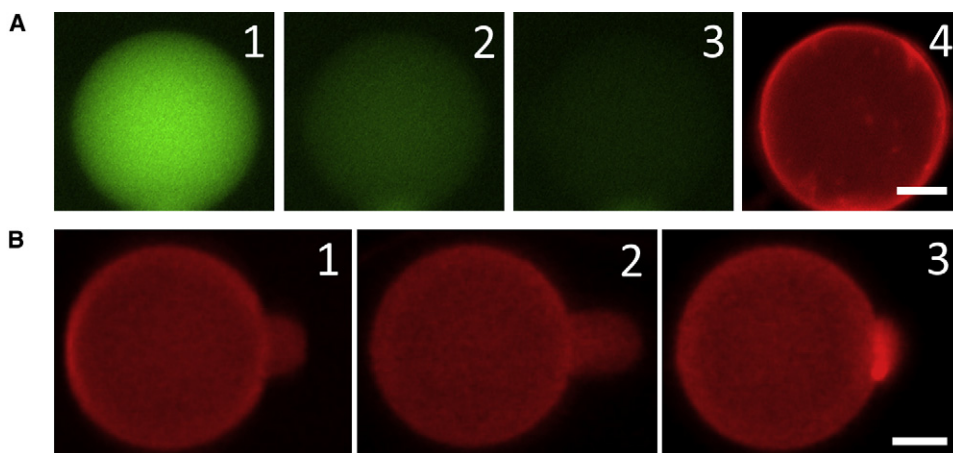

FIGURE 6 (A) GUV with red dye in the lipid and green dye in its content was exposed to 5 μM LL-37. Leakage occurred stochastically. 1) $t = 0$, right before leakage occurred. 2) $t = 30$ s. 3) $t = 60$ s. 4) $t = 300$ s (the GUV was still intact). Within 60 s, the leakage reduced the content dye intensity to ~10% of the $t = 0$ value, whereas photobleaching decreased the intensity of a nonleaking GUV to ~90%. Leakage was complete at $t \sim 200$ s. (B) 1) An aspirated GUV was exposed to 0.5 μM LL-37. 2) The protrusion length initially increased, indicating a membrane area expansion without pore formation (the image shows the maximum protrusion). 3) After reaching the maximum, the protrusion length decreased, indicating pore formation in the membrane (see text). In nine runs of aspiration experiments, the average time to reach the maximum protrusion was ~13 s and the average time to decrease to the original protrusion length (where $\Delta A/A = 0$) was ~10 s. Both scale bars = 10 μm.

pore formation (45). When the fractional area expansion $\Delta A/A$ reached a value of ~1.3%, the protrusion length began to decrease, indicating the formation of pores in the membrane. The decrease of the protrusion length was due to the finite size of the peptide-induced pores, which allowed more permeation of the smaller glucose compared with the larger sucrose, and the resultant osmolality imbalance induced a net water influx. This increase and then decrease of the GUV protrusion has been carefully analyzed with other peptides, with the variations of sugar concentrations and with the exchange of sucrose and glucose (18,29,46,47). The maximum area expansion $\Delta A/A$ of GUVs can be directly related to a critical peptide concentration P/L*: $(\Delta A/A)_{max} = (P/L)*(A_P/A_L)$ (18). From the values of $(\Delta A/A)_{max}$, A_P, and A_L, we obtained P/L*~1/320. This is the critical P/L value. When the P/L of the peptides adsorbed to the bilayer was below P/L*, the bound peptides expanded the membrane area without pore formation. Further binding of the solution peptides to the GUV made P/L exceed P/L*, and then the peptides began to form pores. This P/L* value for LL-37 in DOPC is too small to be measured in equilibrium experiments. For the peptides or the effect of peptides in stacked membranes to be detectable by OCD or x-ray/neutron techniques, the P/L must be ~$\geq$1/150. For example, for melittin in di20:1PC (P/L*~1/70) and di22:1PC (P/L*~1/40), the same value of P/L* was obtained in both kinetic and equilibrium experiments (18).

The structural data obtained from stacked membranes of peptide-lipid mixtures corroborated the GUV findings. When the P/L of the peptide-lipid mixture was above P/L*, a substantial fraction of the LL-37 peptides became embedded in the bilayer with their helical axes normal to the plane of the bilayer, consistent with pore formation. A surprising finding was that the normal orientation of LL-37 helices was observed only in swollen states, with a D spacing exceeding ~70 Å, and not in the same stacked membranes fully hydrated by ~100% RH water vapor, which had a D spacing ~52 Å, or in any drier condition. We assume that stacked membranes at larger D spacings are closer to the situation in which peptides interact with bilayer membranes in solution.

In swollen states with P/L > P/L*, neutron scattering revealed LL-37 forming transmembrane pores in lipid bilayers with a water channel, but no pores were detected under nonswollen conditions. Because the primary purpose of this investigation was to determine whether LL-37 forms pores, we only measured LL-37 in DOPC bilayers in two P/L values (1/100 and 1/50). Pores were detected in both cases, with the water channel radius at 23 and 33 Å, respectively. Much more systematic neutron studies were carried out for the pores formed by smaller peptides, i.e., alamethicin (21), magainin (35), melittin (34), and protegrin (28). We analyzed, and confirmed by anomalous x-ray diffraction, two types of peptide-induced transmembrane pores: the barrel-stave pore and the toroidal pore (34,38,39). Only the special peptide alamethicin, which is electrically neutral and barely soluble in water, forms barrel-stave pores. All other peptides (which are highly cationic and water-soluble) form toroidal pores. The toroidal pores of magainin, melittin, and protegrin have water channel radii in the range of 15–25 Å, and vary in size depending on the P/L ratio and lipid composition (35). The toroidal pores are substantially larger than the barrel-stave pores of alamethicin, which have a water channel radius of 9 Å (21). The pores formed by LL-37 are characteristic of the toroidal type. The GUV experiments are consistent with LL-37 binding on the membrane surface at low P/L ratios and forming transmembrane pores at high P/L ratios. Its mechanism is consistent with the two-state model exhibited by magainin and protegrin (17).

Human cathelicidin LL-37 is a widely expressed archetypal AMP (1). Recently, the activity of the Alzheimer's disease-associated amyloid β-protein against microbial organisms was compared with the microbicidal activity of LL-37 (50). It is significant that despite the versatile multifunctionality of LL-37, our experimental results suggest that its molecular mechanism for direct antimicrobial activity may be similar to that of smaller AMPs such as magainin and protegrin. Finally, we wonder whether the necessity of studying LL-37 in swollen states implies that a similar consideration should be applied to other large membrane-active peptides and proteins.

REFERENCES

1. Zanetti, M. 2004. Cathelicidins, multifunctional peptides of the innate immunity. *J. Leukoc. Biol.* 75:39–48.

2. Turner, J., Y. Cho, …, R. I. Lehrer. 1998. Activities of LL-37, a cathelin-associated antimicrobial peptide of human neutrophils. *Antimicrob. Agents Chemother.* 42:2206–2214.

3. Scott, M. G., D. J. Davidson, …, R. E. Hancock. 2002. The human antimicrobial peptide LL-37 is a multifunctional modulator of innate immune responses. *J. Immunol.* 169:3883–3891.

4. Koczulla, R., G. von Degenfeld, …, R. Bals. 2003. An angiogenic role for the human peptide antibiotic LL-37/hCAP-18. *J. Clin. Invest.* 111:1665–1672.

5. Zaiou, M. 2007. Multifunctional antimicrobial peptides: therapeutic targets in several human diseases. *J. Mol. Med.* 85:317–329.

6. De, Y., Q. Chen, …, O. Chertov. 2000. LL-37, the neutrophil granule- and epithelial cell-derived cathelicidin, utilizes formyl peptide receptor-like 1 (FPRL1) as a receptor to chemoattract human peripheral blood neutrophils, monocytes, and T cells. *J. Exp. Med.* 192:1069–1074.

7. Zasloff, M. 2002. Antimicrobial peptides of multicellular organisms. *Nature.* 415:389–395.

8. Oren, Z., J. C. Lerman, ..., Y. Shai. 1999. Structure and organization of the human antimicrobial peptide LL-37 in phospholipid membranes: relevance to the molecular basis for its non-cell-selective activity. *Biochem. J.* 341:501–513.

9. Porcelli, F., R. Verardi, ..., G. Veglia. 2008. NMR structure of the cathelicidin-derived human antimicrobial peptide LL-37 in dodecylphosphocholine micelles. *Biochemistry.* 47:5565–5572.

10. Henzler Wildman, K. A., D. K. Lee, and A. Ramamoorthy. 2003. Mechanism of lipid bilayer disruption by the human antimicrobial peptide, LL-37. *Biochemistry.* 42:6545–6558.

11. Sood, R., Y. Domanov, ..., P. K. Kinnunen. 2008. Binding of LL-37 to model biomembranes: insight into target vs host cell recognition. *Biochim. Biophys. Acta.* 1778:983–996.

12. Caillé, A. 1972. Physique cristalline: remarques sur la diffusion des rayons X dans les smectiques A. *C. R. Acad. Sci. Paris Ser. B.* 274:891–893.

13. Lei, N., C. R. Safinya, and R. F. Bruinsma. 1995. Discrete harmonic model for stacked membranes: theory and experiment. *J. Phys. II.* 5:1155–1163.

14. Safinya, C. R., D. Roux, ..., A. M. Bellocq. 1986. Steric interactions in a model multimembrane system: a synchrotron X-ray study. *Phys. Rev. Lett.* 57:2718–2721.

15. Wack, D. C., and W. W. Webb. 1989. Measurement by X-ray diffraction methods of the layer compressional elastic constant B in the lyotropic smectic-A (L-α) phase of the lecithin-water system. *Phys. Rev. A.* 40:1627–1636.

16. Wu, Y., H. W. Huang, and G. A. Olah. 1990. Method of oriented circular dichroism. *Biophys. J.* 57:797–806.

17. Huang, H. W. 2000. Action of antimicrobial peptides: two-state model. *Biochemistry.* 39:8347–8352.

18. Lee, M. T., W. C. Hung, ..., H. W. Huang. 2008. Mechanism and kinetics of pore formation in membranes by water-soluble amphipathic peptides. *Proc. Natl. Acad. Sci. USA.* 105:5087–5092.

19. Ludtke, S., K. He, and H. Huang. 1995. Membrane thinning caused by magainin 2. *Biochemistry.* 34:16764–16769.

20. Yang, L., and H. W. Huang. 2003. A rhombohedral phase of lipid containing a membrane fusion intermediate structure. *Biophys. J.* 84:1808–1817.

21. He, K., S. J. Ludtke, ..., H. W. Huang. 1996. Neutron scattering in the plane of membranes: structure of alamethicin pores. *Biophys. J.* 70:2659–2666.

22. Powers, L., and P. S. Pershan. 1977. Monodomain samples of dipalmitoyl phosphatidylcholine with varying concentrations of water and other ingredients. *Biophys. J.* 20:137–152.

23. Ladokhin, A. S., and S. H. White. 2004. Interfacial folding and membrane insertion of a designed helical peptide. *Biochemistry.* 43:5782–5791.

24. Burck, J., S. Roth, ..., A. S. Ulrich. 2008. Conformation and membrane orientation of amphiphilic helical peptides by OCD. *Biophys. J.* 95:3872–3881.

25. Cheng, J. T., J. D. Hale, ..., S. K. Straus. 2009. Effect of membrane composition on antimicrobial peptides aurein 2.2 and 2.3 from Australian southern bell frogs. *Biophys. J.* 96:552–565.

26. Lynn, G. W., W. T. Heller, ..., D. A. Myles. 2006. Bio-SANS—a dedicated facility for neutron structural biology at Oak Ridge National Laboratory. *Condens. Matter.* 385–386:880–882.

27. Lee, C. C., Y. Sun, and H. W. Huang. 2010. Membrane-mediated peptide conformation change from α-monomers to β-aggregates. *Biophys. J.* 98:2236–2245.

28. Yang, L., T. M. Weiss, and H. W. Huang. 2000. Crystallization of antimicrobial pores in membranes: Magainin and protegrin. *Biophys. J.* 79:2002–2009.

29. Sun, Y., W. C. Hung, ..., H. W. Huang. 2009. Interaction of tea catechin (-)-epigallocatechin gallate with lipid bilayers. *Biophys. J.* 96: 1026–1035.

30. Chen, F. Y., W. C. Hung, and H. W. Huang. 1997. Critical swelling of phospholipid bilayers. *Phys. Rev. Lett.* 79:4026–4029.

31. Johansson, J., G. H. Gudmundsson, ..., B. Agerberth. 1998. Conformation-dependent antibacterial activity of the naturally occurring human peptide LL-37. *J. Biol. Chem.* 273:3718–3724.

32. Terwilliger, T. C., L. Weissman, and D. Eisenberg. 1982. The structure of melittin in the form I crystals and its implication for melittin's lytic and surface activities. *Biophys. J.* 37:353–361.

33. Fox, Jr., R. O., and F. M. Richards. 1982. A voltage-gated ion channel model inferred from the crystal structure of alamethicin at 1.5-A resolution. *Nature.* 300:325–330.

34. Yang, L., T. A. Harroun, ..., H. W. Huang. 2001. Barrel-stave model or toroidal model? a case study on melittin pores. *Biophys. J.* 81: 1475–1485.

35. Ludtke, S. J., K. He, ..., H. W. Huang. 1996. Membrane pores induced by magainin. *Biochemistry.* 35:13723–13728.

36. Yang, L., T. A. Harroun, ..., H. W. Huang. 1998. Neutron off-plane scattering of aligned membranes. I. Method of measurement. *Biophys. J.* 75:641–645.

37. Yang, L., T. M. Weiss, ..., H. W. Huang. 1999. Supramolecular structures of peptide assemblies in membranes by neutron off-plane scattering: method of analysis. *Biophys. J.* 77:2648–2656.

38. Qian, S., W. Wang, ..., H. W. Huang. 2008. Structure of transmembrane pore induced by Bax-derived peptide: evidence for lipidic pores. *Proc. Natl. Acad. Sci. USA.* 105:17379–17383.

39. Qian, S., W. Wang, ..., H. W. Huang. 2008. Structure of the alamethicin pore reconstructed by X-ray diffraction analysis. *Biophys. J.* 94: 3512–3522.

40. Mecke, A., D. K. Lee, ..., M. M. Banaszak Holl. 2005. Membrane thinning due to antimicrobial peptide binding: an atomic force microscopy study of MSI-78 in lipid bilayers. *Biophys. J.* 89:4043–4050.

41. Pabst, G., S. Danner, ..., J. Katsaras. 2007. Entropy-driven softening of fluid lipid bilayers by alamethicin. *Langmuir.* 23:11705–11711.

42. Huang, H. W. 2009. Free energies of molecular bound states in lipid bilayers: lethal concentrations of antimicrobial peptides. *Biophys. J.* 96:3263–3272.

43. Lee, M. T., F. Y. Chen, and H. W. Huang. 2004. Energetics of pore formation induced by membrane active peptides. *Biochemistry.* 43:3590–3599.

44. Tamba, Y., and M. Yamazaki. 2005. Single giant unilamellar vesicle method reveals effect of antimicrobial peptide magainin 2 on membrane permeability. *Biochemistry.* 44:15823–15833.

45. Kwok, R., and E. Evans. 1981. Thermoelasticity of large lecithin bilayer vesicles. *Biophys. J.* 35:637–652.

46. Longo, M. L., A. J. Waring, ..., D. A. Hammer. 1998. Area expansion and permeation of phospholipid membrane bilayer by influenza fusion peptides and melittin. *Langmuir.* 14:2385–2395.

47. Sun, Y., C. C. Lee, ..., H. W. Huang. 2008. The bound states of amphipathic drugs in lipid bilayers: study of curcumin. *Biophys. J.* 95:2318–2324.

48. Tamba, Y., H. Ariyama, ..., M. Yamazaki. 2010. Kinetic pathway of antimicrobial peptide magainin2 induced pore formation in lipid membranes. *J. Phys. Chem. B.* 114:12018–12026.

49. Fuertes, G., A. J. Garcia-Saez, ..., J. Salgado. 2010. Pores formed by baxα5 relax to a smaller size and keep at equilibrium. *Biophys. J.* 99:2917–2925.

50. Soscia, S. J., J. E. Kirby, ..., R. D. Moir. 2010. The Alzheimer's disease-associated amyloid β-protein is an antimicrobial peptide. *PLoS ONE.* 5:e9505.